# VISUALIZATION OF PHYSICAL PROCESSES IN LIQUID DROPS ON HORIZONTAL SURFACE

I.N. PAVLOV[c], B.S. RINKEVICHYUS, A.V. TOLKACHEV

National Research University "Moscow Power Engineering Institute", V.A. Fabrikant Physics Department, Krasnokazarmennaya str., 14, 111250, Moscow, Russia

[c]Corresponding author: Email: inpavlov@bk.ru

**KEYWORDS**:

**Main subjects**: liquid drop

**Fluid:** liquid drops evaporation

**Visualization method(s):** frustrated total internal reflection, interferometry

**Other keywords:** evanescent waves

**ABSTRACT**: This paper describes the application of the method of frustrated total internal reflection (FTIR) for the visualization of the processes taking place during evaporation, cooling, and spreading of a liquid droplet on a horizontal substrate. An experimental setup is created, whose operating principle is based on the FTIR phenomenon. Experiments are conducted on the visualization of the processes of evaporation, cooling, spreading, and crystallization of a drop of liquid on a horizontal substrate. The results of modeling the interference patterns obtained are presented.

**INTRODUCTION**: The problem of evaporation of a liquid droplet into the surrounding gas is a classical problem for physics; its solution has been the subject of investigation by many scientists. Nevertheless, it has not lost its urgency to this day because of the emergence of new possibilities for its application, including the manufacture of nanomaterials, studies into the extension of DNA molecules, imaging of DNA molecules, protein crystallization methods, development of printing techniques for ink-jet printers, and a number of other applications [1]. In this connection, a demand has arisen for the development of novel methods for studying evaporation of liquid droplets.

The growing interest in the self-organization processes in drying droplets of multicomponent liquids [2] has lately generated a need for the development and application of various techniques for diagnosing these processes. The study of the evaporation of a liquid droplet by the usual method using a microscope allows obtaining only information about the shape of the droplet, but is incapable of providing information about the contact layer between the droplet and the substrate surface. In this work, to visualize the process of evaporation of a liquid droplet, use is made of the frustrated total internal reflection (FTIR) method that has earlier been successfully employed to visualize nonuniform near-wall liquid flows in a cell and flat and T-shaped microchannels [3–5].

**METHODS**: The method suggested here for the visualization of evaporation of liquid droplets is based on the FTIR phenomenon, and so it allows recording small variations of the refractive index of the droplet of interest in a thin layer on the order of a few hundreds of nanometers in thickness near the substrate surface. The method is essentially as follows. A droplet of liquid with a refractive index of $n_l$ is placed on the horizontal interface between a glass prism with a refractive index of $n_g$ and air whose refractive index is $n_a$, whereon the droplet dries up. This surface of the prism is illuminated from below with a broad parallel laser beam incident at an angle of $\theta_i$ greater than the critical angle of total internal reflection (TIR) for the glass-to-air interface, but smaller than that for the glass-to-liquid interface; i.e, $n_a/n_g < \sin\theta_i < n_l/n_g$. Since the TIR condition for the liquid is not satisfied, the reflection coefficient for the part of the beam reflected from the glass-to-liquid interface is lower than that for the part of the beam reflected from the glass-to-air interface (this reflection coefficient is equal to unity). The case where the polarization of the incident beam is parallel to the plane of incidence [3] is optimal from the standpoint of the sensitivity of the method; therefore, it is precisely this case that is considered in the subsequent discussion. In that case, the energetic reflection coefficient is defined by the formula

$$\rho_{||} = \tan^2\left[\theta_i - \arcsin\left(\frac{n_g}{n_l}\sin\theta_i\right)\right] / \tan^2\left[\theta_i + \arcsin\left(\frac{n_g}{n_l}\sin\theta_i\right)\right], \quad (1)$$

where $\theta_i$ is the incidence angle of the laser beam, $n_g$ is the refractive index of glass, and $n_l$ is the refractive index of the liquid droplet.

For this reason, observed in reflected light is a dark image of the droplet against the bright background of the beam reflected from the glass-to-air interface. Visualized in this way are the position of the droplet and its size. By measuring the coefficient $\rho_{||}$ of reflection from the droplet for the given incidence angle $\theta_i$, one can estimate the

refractive index $n_l$ of the liquid. Figure 1 shows the reflection coefficient of a liquid as a function of its refractive index for different beam incidence angle $\theta_i$.

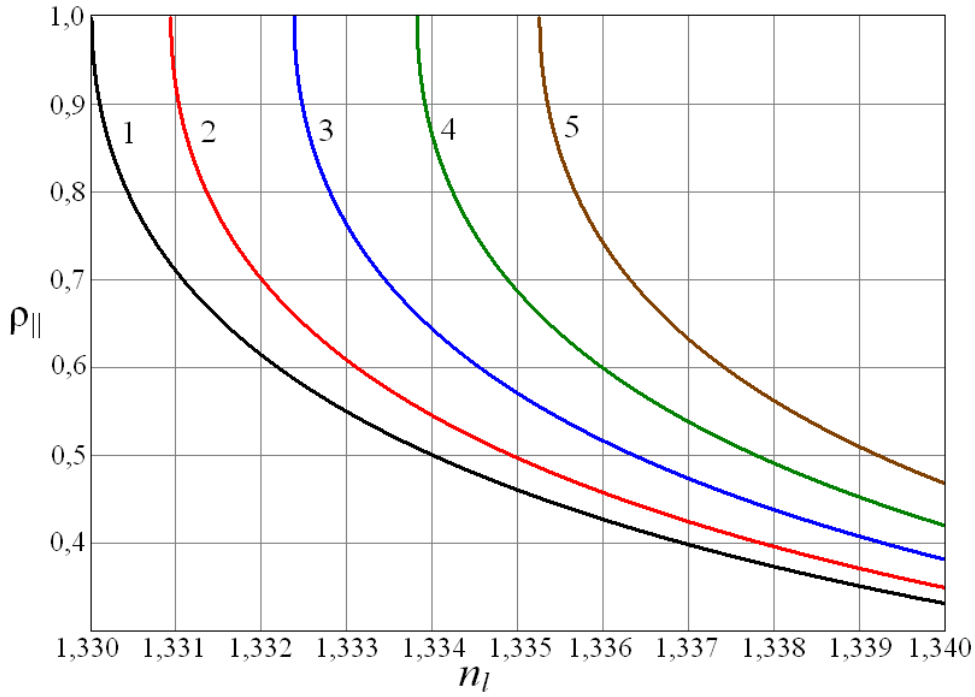


Fig. 1. Reflection coefficient of a liquid as a function of its refractive index:
1 – $\theta_i$ = 58.036°; 2 – $\theta_i$ = 58.1°; 3 – $\theta_i$ = 58.2°; 4 – $\theta_i$ = 58.3°

It can be seen from the figure that the method has a high sensitivity in terms of refractive index in the neighborhood of the critical angle for total internal reflection.

The method can be implemented with both incoherent radiation and coherent laser radiation. In the case of coherent laser radiation, the actual reflection coefficient is difficult to determine because the rays repeatedly reflected from the external surface of the liquid droplet interfere with the rays reflected from the surface of the prism, so that observed on the screen is not the intensity distribution corresponding to the reflection coefficient for the given refractive indices, but an interference pattern.

When processing interference patterns obtained on refraction FTIR images, use was made of the following assumptions. The shape of the droplet surface reflecting the rays passing through the interface was taken to be spherical with a large radius of curvature. By analogy with calculations for Newton's rings, all the rays reflected from this surface were assumed to remain parallel as in the incident beam, with the shape of the surface affecting only the difference in path length between them. Figure 2 shows the paths of the interfering rays. The ray *a* gets into the prism, crosses the prism-to-liquid interface at the point *A*, and reflects from the outer surface of the droplet at the point *B*. Next it meets at the point *C* with the ray *b* reflected from the prism-to-liquid interface. Since it is laser radiation that is used here, these rays interfere with each other.

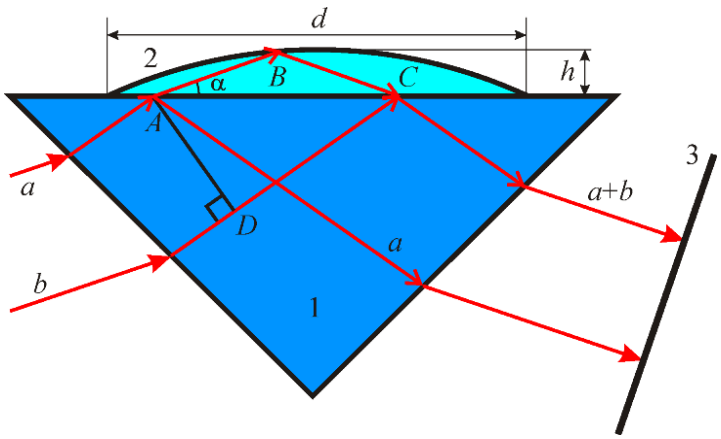


Fig. 2. Paths of the interfering rays *a* and *b* in a liquid droplet placed on the surface of a prism: *1* –prism; *2* – liquid droplet; 3 – screen

By simple manipulations, we get the following formula for the difference in path length $\Delta l$ between the interfering rays *a* and *b*:

$$\Delta l = (AB + BC)\cdot n_l - (DC)\cdot n_g,\ \ AB + BC = \tilde{n} - \sqrt{\tilde{n}^2 - 4\cdot\tilde{n}\cdot\xi + 4\cdot\frac{d^2 - \eta^2}{\cos\alpha}},\ \ \tilde{n} = \frac{d^2\cdot\tan\alpha}{h\cdot\cos\alpha}, \qquad (2)$$

where ξ, η are coordinates in the plane of the interface, *d* is the diameter of the droplet, *h* is its height, and α is the angle between the ray refracted in the droplet and the interface.

The light intensity distribution in the interference pattern is described by the expression

$$I(x,y) = I_1 + I_2 + 2\sqrt{I_1 I_2}\cos\Delta\varphi, \qquad (3)$$

where $\Delta\varphi = (2\pi/\lambda_0)n_l\Delta l$, $\lambda_0$ is the radiation wavelength in vacuum, $I_1$ is the intensity of the ray *a* on the screen, and $I_2$ is the intensity of the ray *b* on the screen (in the general case, $I_1 \neq I_2$).

Figure 3 presents an interference pattern obtained through modeling by the above formula for $d$ = 3.75 mm, $h$ = 0.01 mm, α = 5°, and $\lambda_0$ = 0.6 μm.

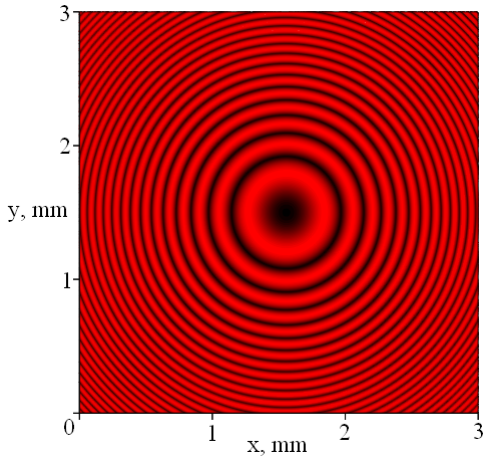


Fig. 3. Modeled interference pattern in the beams reflected from the liquid droplet

It should be noted that the use of FTIR methods makes it possible to investigate the bottom contact layer of the droplet, whereas other methods, for example, the laser refractography [6] and the background-oriented schlieren method [7] allows determining the shape of the surface of the evaporating liquid droplet.

**EXPERIMENTAL SETUP**: A schematic diagram of the experimental setup is presented in Figure 4. The radiation source here is a semiconductor laser 3 mW in power and 655 nm in radiation wavelength. The optical system for forming a broad collimated laser beam 40 mm in diameter consists of two lenses differing in focal length and a spatial filter – a pinhole aperture. The rectangular glass prism with a refractive index of $n_g$ = 1.5677 for a wavelength of λ = 655 nm is held to a coordinate table that allows it to be moved vertically in order that the laser beam can be made to fall at the center of its base, no mater what the beam incidence angle. The receiving part fixed on the other arm of

device consists of a ground glass screen and a digital video camera capable of taking 8-bit images with a resolution of 1392×1040 pixels at a rate of 7 frames per second. Installed on the personal computer is an application package for the digital recording and processing of the refractographic images obtained. The radiation from laser *1* passes through a beam expander optical system comprising a telescopic system of two collecting lenses differing in focal length and a spatial filter in the form of a pinhole aperture. The expanded collimated laser beam passes through the side face of prism *3* and reflects from its base that serves as a substrate for evaporating liquid drop *4*. The angle of reflection corresponds to the TIR condition for the prism-to-air interface. The reflected beam falls on diffuse scattering screen *5*, and the image thereon is recorded with CCD camera *6* and then processed on personal computer *7*.

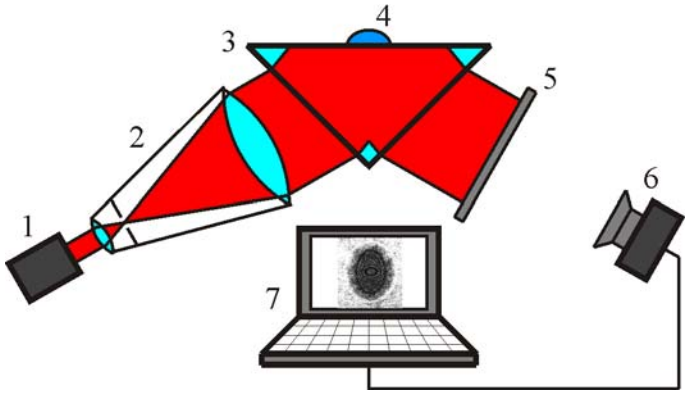


Fig. 4. Schematic diagram of the experimental setup: *1* – laser; *2* – beam expander; *3* – prism; *4* – liquid droplet; *5* – screen; *6* – CCD camera; *7* – personal computer

The setup can be operated in two modes – refraction and interference ones, depending on the incidence angle of the laser beam. At a great beam incidence angle (close to the critical TIR angle) the setup operated in the refraction mode can perceive a change of the refractive index of a liquid accurate to three decimal places. In its interference mode at a smaller beam incidence angle, the setup enables one to determine the evaporation dynamics of the liquid with a resolution of $\lambda/2$. The appearance of the setup is presented in Fig. 5.

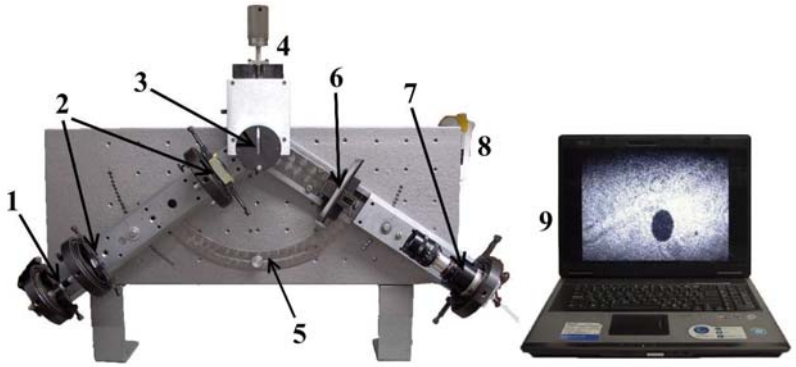


Fig. 5. Photograph of the experimental setup: *1* – laser; *2* – optical system; *3* – prism; *4* – coordinate table; *5* – beam incidence angle adjustment device; *6* – screen; *7* – video camera; *8* – microdispenser; *9* – personal computer

**RESULTS**: The above-described setup was used to conduct experiments on the visualization of the processes of evaporation, spreading, cooling, and crystallization of droplets of various liquids.

Figure 6 presents some examples of experimental images obtained with this setup for beam incidence angles smaller than the critical TIR angle for the prism-to-liquid interface. The liquids studied include isopropyl alcohol, ethyl alcohol, a solvent, acetone, and aqueous solutions of common salt and sugar. The time analysis of changes taking place in these interference patterns provides extensive information on the evaporation dynamics of liquid droplets on a solid surface. The distortions of the shape of interference rings are due to the deviation of the form of the droplet surface from the spherical one. The rate of motion of the rings characterizes the evaporation rate of the droplet.

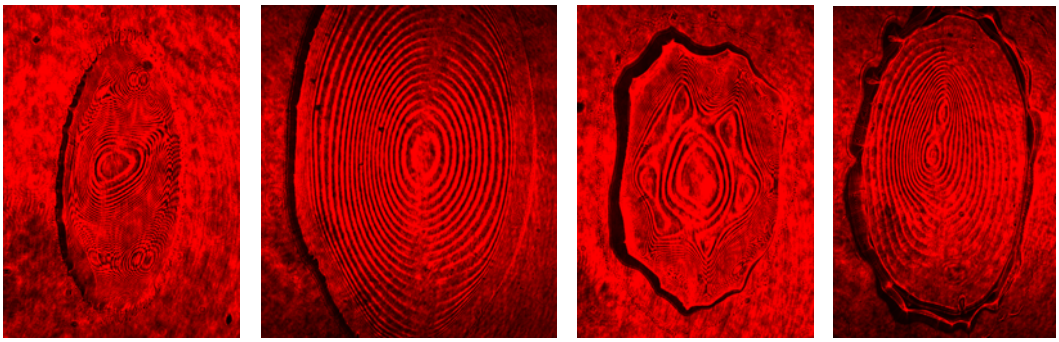

a) b) c) d)

Fig. 6. Examples of interference images of evaporating liquid droplets: (*a*) isopropyl alcohol; (*b*) solvent; (*c*) acetone; (*d*) ethyl alcohol

The experiments on the visualization of evaporation of various liquid droplets were performed under different conditions: subject to variation were the laser beam incidence angle, the substrate surface roughness, the volume of the droplet, and its temperature. Some examples of images obtained in this case are presented in Fig. 7. The image of Fig. 7*a* was obtained by recording from the screen, while those of Figs. 7*b* and *c*, by recording directly from the surface of the prism.

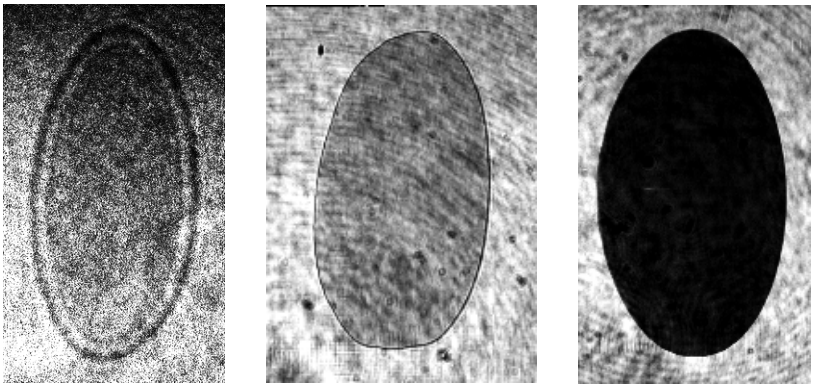

a) b) c)

Fig. 7. Refractographic image of a water droplet: (*a*) and (*b*) at a beam incidence angle close to the critical TIR angle; (*c*) in the case of total internal reflection

When visualizing the cooling of a droplet of hot water on the surface of the prism, the beam incidence angle was close to the critical TIR angle, and so no interference rings were observed. When processing the images obtained, we got matrices of the contrast coefficient $M = 1 - \rho_{||}$, where $\rho_{||}$ is the energetic coefficient of reflection of the incident radiation. To this end, we took two images: the base image obtained without the droplet and the refractographic image of the droplet. We next subtracted the latter image from the former one, and normalized the brightness values of the pixels in the resultant image to those in the base image. A matrix was thus obtained of the contrast coefficients at each point of the image, whose size coincided with the resolution of the latter. Some examples of relationship between the contrast coefficient and the coordinate along the center section of a hot liquid droplet are presented in Fig. 8. These curves were obtained for two instants of the droplet cooling time: (*1*) in the beginning of the process 2 seconds after the droplet was placed on the prism and (2) at the end of the process 90 seconds after the placement of the droplet. The initial temperature of the droplet 10 μl in volume was 90 °C. It can be seen from the figure that at the initial instant of time the contrast coefficient in the droplet image was lower than later on. This is due to the fact that as the droplet cools through heat exchange with the surface of the prism and the surrounding medium, its refractive index increases, hence its reflection coefficient decreases, while the contrast coefficient, on the contrary, grows higher.

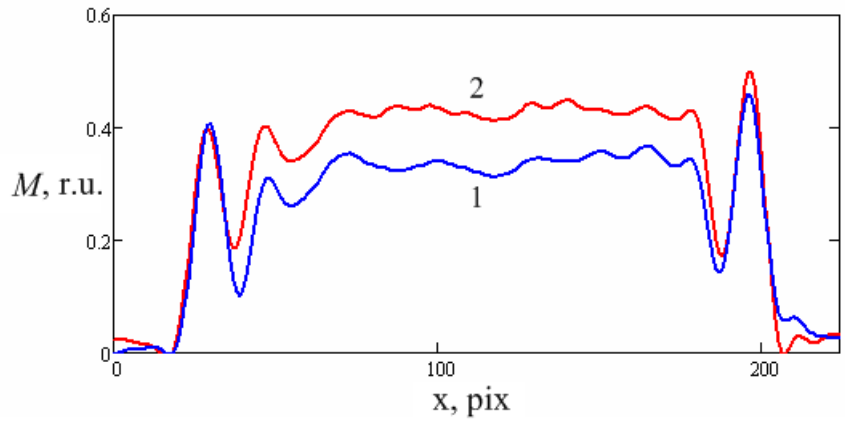


Fig. 8. Contrast coefficient $M$ as a function of the coordinate $x$ for two instants of time: $t_2 > t_1$

Experimental studies were also conducted into the process of spreading of a liquid droplet on various surfaces differing in roughness. The surfaces used were the bases of prisms ground with grinding powders differing in grain size: M-28 (prism №1), M-14 (prism №2), and M-7 (prism №3). Also the prism with standard optical surface was used (prism №4). The subject of study was the dynamic condition of the droplet following its placement on the substrate surface. The droplet was formed by means of a microdispenser rigidly fixed on the experimental setup over the prism so that the distance between the nosepiece of the microdispenser and the surface of the prism was 8 mm. The characteristic times of the droplet contact spot size variation amount to a few tens of milliseconds, and therefore to record the images, use was made of a Model HiSpec 2G Mono (Fastec Imaging) high-speed camera. The camera was focused onto the liquid droplet placed on the surface of the prism. The incidence angle of the laser radiation was greater than the TIR angle for the prism-to-air interface, but smaller than that for the prism-to-liquid interface in the case of smooth surface, where the dark image of the droplet appeared against a bright background. The images were recorded at a frequency of 1500 Hz. Some examples of images of a distilled water droplet spreading over the surface of a glass prism are presented in Fig. 9. The images of Fig. 9*a* were obtained with a prism having a smoothly polished base surface (prism №4), while those of Fig. 9*b* are for a prism with its base surface ground with a Grade M-7 grinding powder (prism №3). The images obtained were processed and thereafter time dependences were constructed for the contact spot surface area of the droplet (Fig. 10).

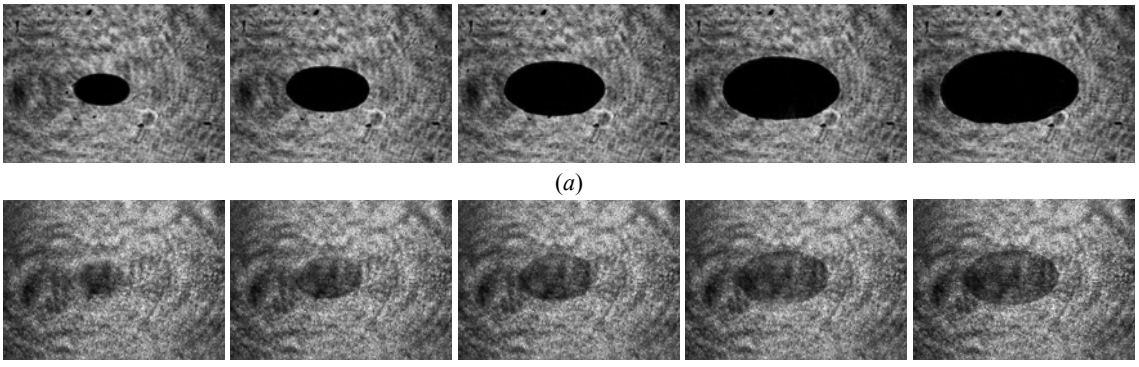

(*a*)

(*b*)

Fig. 9. Spreading of a water droplet over the surface of a glass prism: (a) prism №4 and (*b*) prism №3

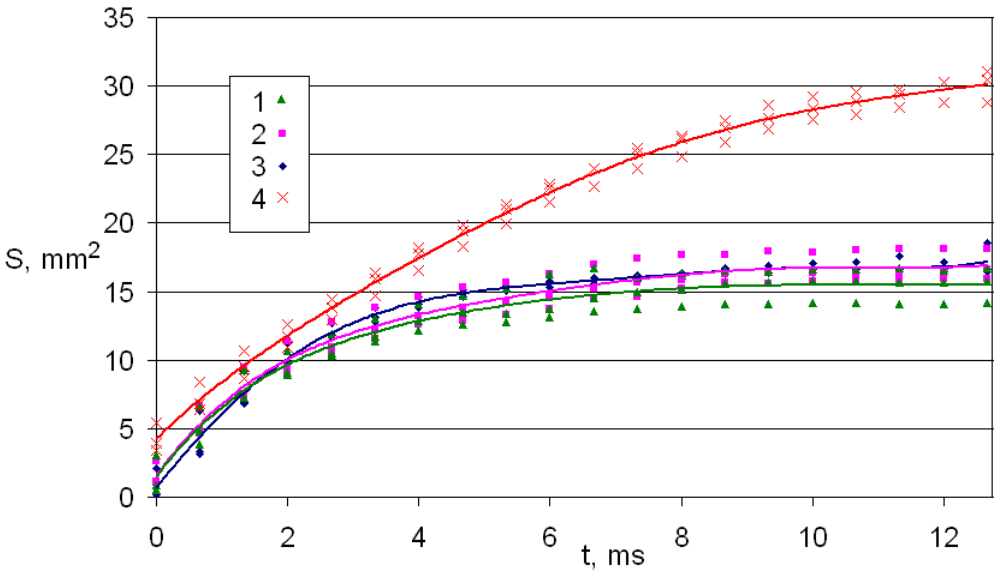


Fig. 10. Contact spot surface area of a water droplet as a function of time for various glass surfaces differing in roughness: *1* – prism №1; *2* – prism №2; *3* – prism №3; *4* – prism №4

We also performed experiments on the visualization of evaporation of a droplet of sugar solution and crystallization of common salt from a saturated aqueous solution. When visualizing the evaporation of the sugar solution, the angle of incidence of the laser radiation onto the surface of the prism was selected to be equal to the TIR angle for this liquid. Therefore, initially seen on the screen is only the contour of the droplet against a bright background, because the entire beam suffered total internal reflection. As water gradually evaporated from the solution, the refractive index of the droplet increased accordingly, so that the TIR condition got violated, and the image of the droplet grew darker. Some examples of the pertinent images obtained at various instants of time during the course of the evaporation process are presented in Fig. 11. By calculating the coefficient of contrast between the intensities of the totally and nontotally internally reflected light, one can determine the time dependence of the refractive index at each point of the image, as well as the refractive index distribution over the contact spot surface of the droplet for a single instant of time.

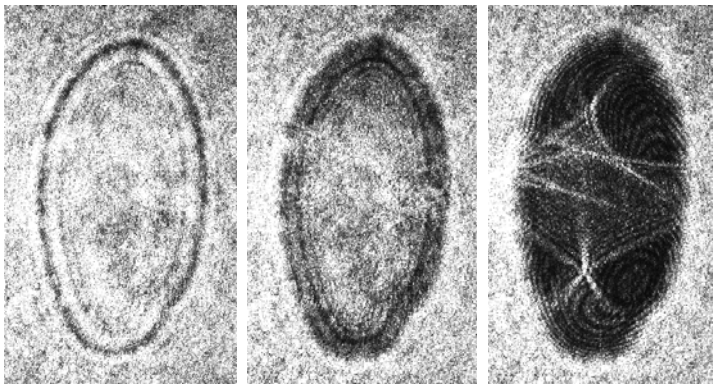

(*a*) (*b*) (*c*)

Fig. 11. Refractographic images of a sugar solution droplet obtained during the course of its evaporation at (*a*) the beginning, (*b*) the middle, and (*c*) the end of the process

The crystallization of common salt from a saturated solution was visualized both by the frustrated total internal reflection method and by direct photographing with a camera from above. The experiments revealed a specific feature consisting in that no traces of the TIR condition being violated by the salt crystals formed remained visible on the screen at the end of the crystallization process. When directly observed from above, the crystallization process taking place upon the drying of the saline solution droplet appears as follows. A few small salt crystals first form at the edges of the droplet. Thereafter they start growing and drawing nearer to the center of the droplet, no fresh crystals

being formed in the process. The crystals eventually draw together close enough to form a ring around the center of the droplet. Throughout this process the size of the contact spot of the droplet remains unchanged; it is only the height of the droplet that is being reduced. Once the height of the droplet has reached a certain value, its size begins decreasing, first at the edges and then inside the ring formed by the crystals. Water remains only beneath the crystals, whence it evaporates for an appreciable length of time. While water is still incompletely evaporated, traces of the TIR condition being violated remain visible in reflected laser light on the screen of the experimental setup. As soon as water evaporates completely, these traces vanish.

**RESULTS**: Our experimental setup relying for its operation on the FTIR phenomenon allows diagnosing various parameters of liquid droplets evaporating from the surface of its prism.

First, it enables one to determine the refractive index distribution over the contact spot surface of the droplet accurate not less than three decimal places.

Secondly, by calculating the rate of motion of the rings of the traveling interference pattern, one can determine the dynamics of variation of the height of the droplet with a resolution of $\lambda/2$.

Thirdly, the method used makes it possible to determine the dynamics of variation of the surface area of the contact spot of the droplet.

Besides, worthy of note is the fact that in contrast to the other methods for diagnosing evaporating liquid droplets, the FTIR technique allows investigating precisely the bottom, contact layer of the liquid.

## Acknowledgements

This work was supported in part by the Ministry of Education and Science of the Russian Federation (State contract no. 14.740.11.0594.) and the Russian Foundation for Basic Research (project no. 10-08-00936a).

## References

1. Barash L.Yu., Bigioni T.P., Vinokur V.M., and Shchur L.N. *Evaporation and fluid dynamics of a sessile drop of capillary size* // Phys. Rev. E 79, 046301 (2009)

2. Tarasevich Yu. Yu., Isakova O.P., Vodolazskaya I.V. *Mathematical Modeling of the Processes of Formation and Evolution of Interphase Fronts in Drying Droplets of Multicomponent Liquids* // Self-Organization Processes in Drying Droplets of Multicomponent Liquids: Experiments, Theories, Applications): Proc. Ist International Conference, Astrakhan: Astrakhan University Publishing House, 2010, pp. 7–25

3. Pavlov I.N., Rinkevichyus B.S. and Tolkachev A.V. *Laser Visualizer of Inhomogeneities in Near-Wall Layer of liquid //* Measurement Techniques, Vol. 53, No. 10, pp. 1130-1134, 2011

4. Pavlov I.N., Rinkevichyus B.S. *Inhomogeneous Near-Wall Liquid Flows Visualization by Frustrated Total Internal Reflection of Laser Beam //* Proc. of PSFVIP-8, Moscow, Russia, 2011, paper No. 105

5. Pavlov I. N., Rinkevichyus B. S. *Near-Wall Liquid Flows Visualization on Frustrated Total Internal Reflection* // Optical Memory and Neural Networks (Information Optics), 2009, Vol. 18, No. 4, pp. 322-327

6. Rinkevichyus B.S., Evtikhieva O.A., Raskovskaya I.L. *Laser Refractography*. New-York, Springer, 2011

7. Mikhalev A.S., Skornyakova N.M. *A Refraction System for Studying Evaporation of Liquid Drops from a Solid Surface* // Measurement Techniques, Vol. 53, No. 12, March, 2011, pp. 1337-1341